A comprehensive gyrokinetic description of global electrostatic microinstabilities in a tokamak

J. Chowdhury,[1] R. Ganesh,[1,a)] S. Brunner,[2] J. Vaclavik,[2] L. Villard,[2] and P. Angelino[3]
[1]*Institute for Plasma Research, Bhat, Gandhinagar 382428, India*
[2]*CRPP, Association EURATOM-Confédération Suisse, EPFL, 1015 Lausanne, Switzerland*
[3]*Association Euratom-CEA, CEA/DSM/DRFC, Cadarache, 13108 St. Paul-lez-Durance, France*

(Received 22 October 2008; accepted 22 April 2009; published online 20 May 2009)

It is believed that low frequency microinstabilities such as ion temperature gradient (ITG) driven modes and trapped electron modes (TEMs) are largely responsible for the experimentally observed anomalous transport via the ion and electron channels in a tokamak. In the present work, a comprehensive global linear gyrokinetic model incorporating fully kinetic (trapped and passing) electrons and ions, actual ion to electron mass ratio, radial coupling, and profile variation is used to investigate the ITG driven modes and pure TEMs. These modes are found to exhibit multiscale structures in the presence of nonadiabatic passing electrons. The multiscale structure is related to the large nonadiabaticity of electrons in the vicinity of mode rational magnetic surfaces and leads to reduced mixing length estimates of transport compared to those obtained from adiabatic electron models. © *2009 American Institute of Physics*. [DOI: 10.1063/1.3134022]

I. INTRODUCTION

Anomalous transport in collisionless hot tokamak plasma is believed to be due to drift waves driven by the density and temperature gradients[1,2] of the particles in a magnetically confined plasma. While the turbulent heat flux of ions is believed to be driven by ion temperature gradient (ITG) mode, the electron heat and particle flux, on the other hand, are expected largely to be driven by the trapped electron mode (TEM) in the low magnetic field side of a tokamak on ion scales and by electron temperature gradient (ETG) on electron scales. Enormous effort has been put to understand the underlying physics issues both theoretically and computationally and then to match the predicted transport flux with that observed experimentally. The study of ion transport by ITG mode has started with adiabatic electron model.[3,4] The next step is then to incorporate the nonadiabatic electrons and is achieved in the form of trapped electrons included in the background model. This has extended the study of this class of microinstabilities to the trapped electron coupled ITG mode (ITG-TEM)[5–12] and TEM.[5,13–16] The new models with trapped electrons give growth rate two to three times larger than the adiabatic electron case. At the same time the transport flux is observed to rise substantially. A comparison of gyrofluid[17] and continuum gyrokinetic[18] simulation of transport in a realistic geometry with experiments has been carried out, and the electron, ion thermal diffusivity, and perturbed density fluctuation level are found to exceed the experimental value by factors of more than 2. The reason of this deviation is expected to be due to the *nonlocal* behavior owing to the variation in the plasma gradients. Following this, sophisticated flux ribbon codes have come up with advanced features[19,20] to reduce the discrepancy between experimental and computational results.[21] Kinetic electron simulation with trapped particles using a generalized split weight scheme to δf gyrokinetic particle method is performed in Ref. 22. The result shows significant increase in the ion heat diffusivity in comparison to the adiabatic electron model in line with the increased growth rate. However, the experimentally observed ion diffusivity[23] is much lower than the adiabatic electron level. Thus a more complete gyrokinetic model that treats electrons and ions on the same physics footing with global profile effects is very much sought to address such anomaly.

The major problem with the incorporation of full dynamics of electrons with nonadiabatic passing fraction in a time dependent model is their fast parallel motion. The high mobility of these electrons needs higher resolution in their response time scale and is a formidable task in the presence of full ion dynamics, the issue of which is well discussed in Ref. 24. With advances in computational facilities, significant progress has been achieved to this end to treat the electrons fully kinetically.[20,25,26]

In the present work, we propose a linear global spectral gyrokinetic model that includes the effect of fully nonadiabatic passing and trapped electrons with true ion to electron mass ratio, kinetic resonances, and finite Larmor radius (FLR) effect to all orders and considers density and temperature profile and the respective gradient variations. The results show the role of the fully kinetic electrons which we term as "nonadiabatic" passing electrons on the trapped electron coupled ITG (ITG-TEM) and pure TEM. It is observed that inclusion of nonadiabatic passing electrons influences strongly the growth rate of ITG-TEM and pure TEM and brings fine radial structures of the mode on the mode rational surfaces. A calculation of flux is done based on the mixing length estimation. It predicts transport level below those obtained from adiabatic electron models.

The model discussed here addresses the nonadiabatic contribution due to all the species in a tokamak, namely, passing ions, trapped ions, passing electrons, and trapped

a)Electronic mail: ganesh@ipr.res.in.

electrons. Recently such a study addressing the effect of nonadiabatic passing electrons on the ITG mode has been reported in Ref. 27. Here the results accounting for all the four subgroups of species are presented, which include ITG, ITG-TEM, and TEMs. Our study on ETG mode with nonadiabatic trapped electrons will be reported elsewhere.

To serve our purpose, here we use the electrostatic version of the fully gyrokinetic, fully electromagnetic global linear stability model EM-GLOGYSTO extensively studied and reported in Refs. 5 and 28–34 as applicable to large aspect ratio tokamaks. Thus we drop the parallel and perpendicular magnetic field perturbations, i.e., $B_\perp$ and $B_\parallel$ fluctuations, Shafranov shift, and equilibrium flows. For other details of the EM model, the reader is referred to Refs. 29 and 31. Thus, particle nonadiabaticity for passing ions and trapped ions, passing electrons and trapped electrons, FLR effects to all orders for all species, kinetic resonances, viz., trapped and transit resonances, poloidal and radial coupling of modes due to particle drifts across magnetic flux surfaces are taken into account.

In Sec. II we highlight the main equations. Section III A contains the numerical results for ITG with adiabatic electrons (ITG-adiabEl) and ITG-TEM without nonadiabatic passing electrons and new results when ITG-TEM coupled with nonadiabatic passing electrons. Changes in the mode structures and the corresponding effects on the mixing length estimates of ITG-TEM induced transport and on the threshold η_i values for the transition from dominant TEM to dominant ITG modes are obtained. Section III B contains the numerical studies for TEM with and without nonadiabatic passing electrons. This is followed by the presentation of mode structures and then the mixing length estimation of transport due to TEM for both the cases. Conclusions are presented in Sec. IV.

II. MODEL EQUATIONS

In real space $\mathbf{r}$, for species j, the perturbed density can be expressed as due to adiabatic and nonadiabatic responses of the constituting particles. Thus, for our case, the perturbation in density for species j can be expressed as

$$\tilde{n}_j(\mathbf{r};\omega) = -\left(\frac{q_j N}{T_j}\right)\left[\tilde{\varphi} + \int d\mathbf{k}\,\exp(\iota\mathbf{k}\cdot\mathbf{r}) \times \int d\mathbf{v}\frac{f_{M_j}}{N}(\omega-\omega_j^*)(\iota\mathcal{U}_j,\iota\mathcal{T}_j)\tilde{\varphi}(\mathbf{k};)J_0^2(x_{L_j})\right], \tag{1}$$

where the first term on the right hand side corresponds to the adiabatic response, while the second term represents the nonadiabatic response of the particles to a perturbation with all its kinetic effects. Also, q_j and T_j are the charge and temperature for species j, respectively, and N is the equilibrium density. $\omega_j^* = \omega_{nj}[1+\eta_j/2(v_\parallel^2/v_{\mathrm{th}_j}^2-3)+\eta_j v_\perp^2/2v_{\mathrm{th}_j}^2]$, where $\omega_{nj}=(T_j\nabla_n \ln Nk_\theta)/(q_jB)$ is the *diamagnetic drift frequency*; $\eta_j=(d\ln T_j)/(d\ln N)$, $v_\parallel$ and $v_\perp$ represent parallel and perpendicular velocities, respectively, and v_{th_j} is the thermal velocity of species j. $J_0(x_{L_j})$ is the Bessel function of argument $x_{L_j}=k_\perp\rho_{L_j}$, presenting the FLR effect. We consider a local Maxwellian for each species of mass m_j as

$$f_{M_j}(\xi,\psi) = \frac{N(\psi)}{\left(\frac{2\pi T_j(\psi)}{m_j}\right)^{3/2}}\exp\left(-\frac{\xi}{T_j(\psi)/m_j}\right),$$

where $\xi=v^2/2$. Also in Eq. (1) $\mathcal{U}_j$ represents the guiding center propagator for passing particles of type $j=i,e$ and $\mathcal{T}_j$ represents the guiding center propagator for trapped particles of type $j=i,e$, both describing the equilibrium guiding center motion. For details of the propagator for both passing and trapped particles, the reader is referred to Refs. 5, 27, and 33.

Introducing *quasineutrality condition*

$$\sum_j \tilde{n}_j(\mathbf{r};\omega) \simeq 0, \tag{2}$$

one would finally end up with a generalized eigenvalue problem where ω and $\tilde{\varphi}$ are the eigenvalue and eigenvector, respectively, which can then be conveniently solved in Fourier space by Fourier decomposing the potential in Eq. (2) first and then taking Fourier transform to eventually obtain a convolution matrix in Fourier space. With single charged passing ions, electrons along with trapped ions and electrons, we have

$$\sum_{\mathbf{k}'}\sum_{j=i}\hat{\mathcal{M}}^j_{\mathbf{k},\mathbf{k}'}\tilde{\varphi}_{\mathbf{k}'} + \sum_{\mathbf{k}'}\sum_{j=\mathrm{tr}\text{-}i}\hat{\mathcal{M}}^j_{\mathbf{k},\mathbf{k}'}\tilde{\varphi}_{\mathbf{k}'} + \sum_{\mathbf{k}'}\sum_{j=e}\hat{\mathcal{M}}^j_{\mathbf{k},\mathbf{k}'}\tilde{\varphi}_{\mathbf{k}'} + \sum_{\mathbf{k}'}\sum_{j=\mathrm{tr}\text{-}e}\hat{\mathcal{M}}^j_{\mathbf{k},\mathbf{k}'}\tilde{\varphi}_{\mathbf{k}'} = 0.$$

The axisymmetry of the system considered here enables one in the linear analysis to fix the toroidal mode number n so that the notation $\mathbf{k}=(\kappa,m)$ for the wave vector parametrizes the radial wave number κ and the poloidal wave number m. Thus $\mathbf{k}=(\kappa,m)$ and $\mathbf{k}'=(\kappa',m')$. Note that we have four species: nonadiabatic passing ions (i), trapped ions (tr-i), nonadiabatic passing electrons (e), and trapped electrons (tr-e).

A. Diagnostics: Eigenmode-averaged quantities

Simple diagnostics for various physical quantities are computed as averages over the eigenmode. For example, mode-averaged k_θ^2 is computed as

$$\langle k_\theta^2\rangle = \frac{\int d\rho\sum_m\left|\frac{m}{\rho}\varphi_{(k,m)}\right|^2}{\int d\rho\sum_m|\varphi_{(k,m)}|^2}, \tag{3}$$

where quantities with suffix "(k,m)" imply Fourier weights of the corresponding perturbations.

III. RESULTS AND DISCUSSION

The effect of the nonadiabaticity of passing electrons on the ITG mode is explored and discussed in Ref. 27. In the present work, the effect of nonadiabaticity of passing electrons is extended to ITG coupled TEM (ITG-TEM) and to pure TEMs.

TABLE I. Equilibrium profiles and parameters.

Parameters	Equilibrium profiles
B field: $B_0=1.0$ T	N-profile and T-profile:
Temperature: $T_0=T(s_0)=7.5$ keV	$N(s)/N_0=\exp\left[-\frac{a\delta s_n}{L_{n0}}\tanh\left(\frac{s-s_0}{\delta s_n}\right)\right]$,
Major radius: $R=2.0$ m	$T_{i,e}(s)/T_0=\exp\left[-\frac{a\delta s_T}{L_{T0}}\tanh\left(\frac{s-s_0}{\delta s_T}\right)\right]$,
Minor radius: $a=0.5$ m	$\delta s_n=0.35$, $\delta s_T=0.2$ at $s=s_0$
Radius: $s=\rho/a$, $0.01<s<1.0$, $s_0=0.6$	$q(s)=1.25+0.67\ s^2+2.38\ s^3-0.06\ s^4$
$L_{n0}=0.4$ m, $L_{T0}=0.2$ m $\rightarrow \eta_{i,e}(s_0)=2.0$	such that $q(s=s_0)=2.0$;
$\tau(s)=T_e(s)/T_i(s)=1$, $\epsilon_n=L_{n0}/R=0.2$	shear $\hat{s}$ is positive and at $s=s_0$, $\hat{s}=1$

For this purpose, we consider the profiles and parameters in Table I. The equilibrium profiles corresponding to these parameters are shown in Fig. 1. The chosen parameters lead to the value of $\rho^* \equiv \rho_{L_i}(s=s_0)/a \simeq 0.0175$.

A. ITG-TEM

The real frequency ω_r and growth rates γ normalized by $\omega_{d0}=v_{T_i}(s=s_0)\varrho_{L_i}/a^2$ for ITG-TEM are plotted in Fig. 2. Here we have shown (i) ITG-adiabEl (ITG mode with usual adiabatic electron response, i.e., $\tilde{n}/n=e\phi/T_e$) (dashed line for $\tilde{\gamma}$ and solid line for $\tilde{\omega}_r$ marked with square), (ii) ITG-TEM without nonadiabatic passing electrons (dashed line for $\tilde{\gamma}$ and solid line for $\tilde{\omega}_r$ marked with diamond), and (iii) ITG-TEM with the contribution from nonadiabatic passing electrons (dashed line for $\tilde{\gamma}$ and solid line for $\tilde{\omega}_r$ marked with filled circle). It is clear that the ITG-adiabEl mode is destabilized by the trapped electrons. The increase in the growth rate can be attributed to the following facts: (i) the presence of nonideal effects such as magnetic drift resonances,[10] (ii) trapped electrons cannot respond adiabatically to the local variation in the scalar potential and consequently cannot take part in charge cancellation,[11] and (iii) an increase in the real frequency reduces the ion Landau damping leading to an increase in the growth rate.[12] As can be seen, the growth rate peaks at around $k_\theta \rho_{L_i}=0.5$ corresponding to toroidal mode number $n=8$. The plot for ITG-TEM, along with a nonadiabatic contribution from passing electrons, shows opposite effect of reducing the growth rate as compared to ITG-TEM without nonadiabatic passing electrons. However, the growth rate is still at higher value than the ITG-adiabEl mode. Because of the nonadiabatic response of the passing electrons near the $k_\parallel=0$ surfaces to a perturbation, the electrons simply cannot respond and short circuit the charge separation instantaneously because of which the mode gets finite amount of time to grow unstable. This sets the growth rate of ITG-TEM with nonadiabatic passing electrons higher than the ITG-

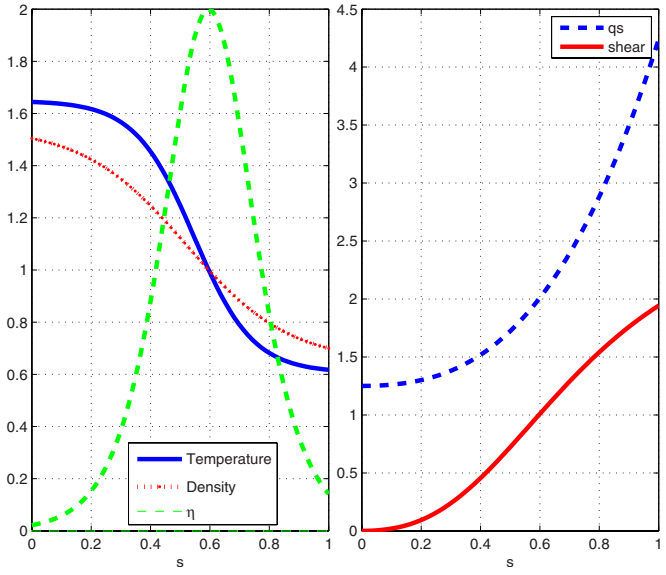

FIG. 1. (Color online) Equilibrium profiles for global ITG stability studies (parameters for Table I). Normalized density, temperature, $\eta_{i,e}$ (left), safety factor q, and magnetic shear $\hat{s}$ profiles as functions of the normalized radius $s=r/a$. Note that η peaks at $s=\rho/a=s_0=0.6$

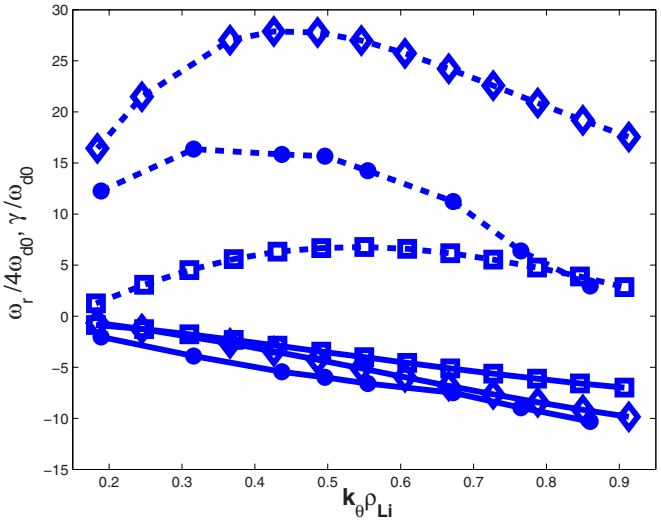

FIG. 2. (Color online) Growth rate $\tilde{\gamma}$ and real frequency $\tilde{\omega}_r$ for $\eta_i(s_0)=2$ (i) for pure ITG with adiabatic electron model (squares), (ii) ITG-TEM without nonadiabatic passing electrons (diamond), and (iii) ITG-TEM with nonadiabatic passing electrons at $\eta_e(s_0)=2.0$ (filled circles).

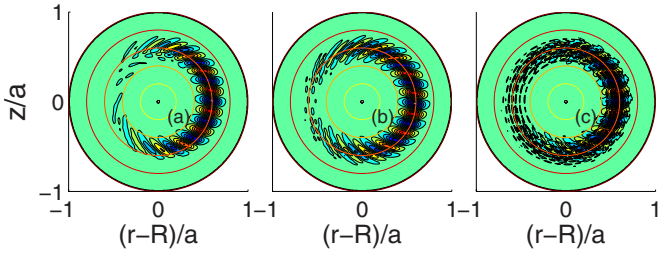

FIG. 3. (Color online) Two dimensional eigenmode structure of global ITG at $n=8$, $\eta_i(s_0)=2$ for (a) pure ITG with adiabatic electrons, (b) ITG-TEM without nonadiabatic passing electrons, and (c) ITG-TEM with nonadiabatic passing electron at $\eta_e(s_0)=2$.

adiabEl mode. The fact that it has growth rate lower than that of the ITG-TEM without nonadiabatic passing electrons can be explained as follows: the inclusion of trapped electrons increases the real frequency of the ITG-adiabEl mode such that there is an upshift of phase velocity $\omega_r/k_\parallel$, making ion Landau resonance regime narrower and thus increasing the growth rate. However, the inclusion of nonadiabatic passing electrons, in addition, increases the real frequency further thereby upshifting the phase velocity more. This makes the mode Landau resonate dominantly with electrons leading to a electron Landau damping of the growth rate. However this damping is not sufficient enough to compensate for the increase in the growth rate produced due to weaker Landau resonance with ions. This can be attributed to the fact that the upshift of the real frequency, when passing nonadiabatic electrons are included, is not drastic, and only a fraction of the electrons resonate with the upshifted phase velocity of the mode. Hence stabilization due to Landau resonance of passing nonadiabatic electrons is weaker than the destabilization due to off-resonance of ions. This sets the growth rate of ITG-TEM with nonadiabatic passing electrons in between the ITG-adiabEl and ITG-TEM without nonadiabatic passing electrons. (For example, reader can see Fig. 6 of Ref. 27.) The corresponding eigenmode structures for the three cases of (i) the ITG-adiabEl mode, (ii) ITG-TEM without nonadiabatic passing electron, and (iii) ITG-TEM with nonadiabatic passing electrons are presented in Fig. 3. The mode structure is quite global so that it can pass through several mode rational surfaces. It reiterates our argument of pronounced nonadiabaticity of passing electrons near the $k_\parallel=0$ surfaces. One can see the changes in the eigenmode structure as one looks from Fig. 3(a) to Fig. 3(c). The mode acquires more

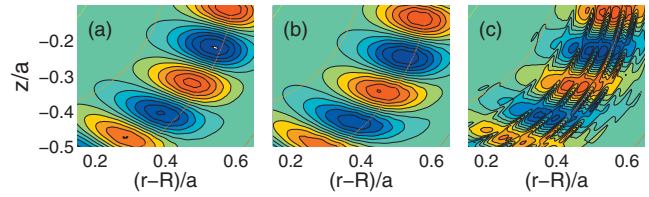

FIG. 4. (Color) Closeup of two dimensional eigenmode structure for (a) pure ITG with adiabatic electrons, (b) ITG-TEM without nonadiabatic passing electrons, and (c) ITG-TEM with nonadiabatic passing electrons at $\eta_e=2(s_0)$.

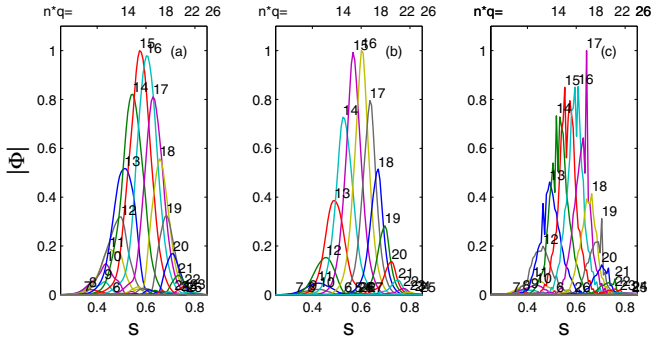

FIG. 5. (Color online) Poloidal Fourier components for electrostatic modes shown in Fig. 3. (a) ITG with adiabatic electrons, (b) ITG-TEM mode without nonadiabatic passing electrons, and (c) ITG-TEM mode with nonadiabatic passing electrons at $\eta_e=2(s_0)$. Note that at each radial location, there are several poloidal harmonics coupled. A few locations where $k_{\parallel m,n}=0$ (i.e., $nq=m$) are indicated on the top axis. Nonadiabatic electrons introduce sharp structure near these points.

and more global nature spreading toward good-curvature region as one goes from case (i) to case (ii) and finally to case (iii).

A close-up look of the eigenmode structures on the poloidal plane is demonstrated in Fig. 4. As can be seen, the inclusion of nonadiabatic passing electrons introduces shorter scales in the eigenmode structures. These electrons near the $k_\parallel=0$ surfaces cannot quench the charge separation by moving along the field lines. So at those surfaces the charge separation leads to stronger EXB drift and pronounced instability. This causes the linear eigenmode structure to break to shorter length scale. The increased strength of the electric field near these surfaces is apparent if one looks at Fig. 5, where the amplitude of the potential corresponding to each poloidal harmonics is documented along the minor radius for the three cases. The position of the mode rational surfaces (where $m=nq$) is shown in the upper axis. Spikes in the potential are visible at those places where $k_\parallel=0$, i.e., at the mode rational surfaces. One can easily see the coupling of poloidal harmonics at each radial location. The corresponding potential amplitudes in the Fourier space is shown in Fig. 6 for (i) the ITG-adiabEl mode, (ii) ITG-TEM

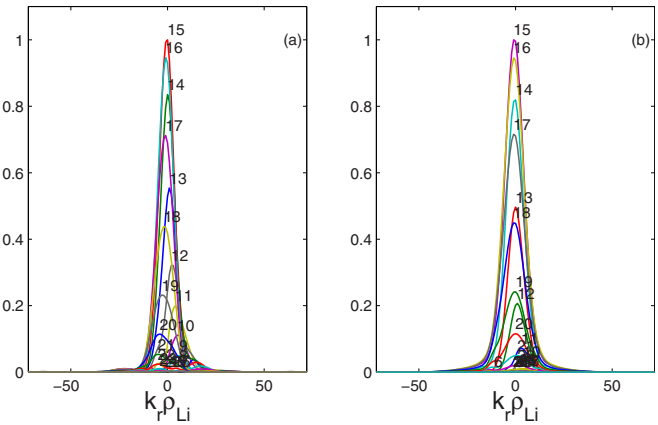

FIG. 6. (Color online) Radial Fourier harmonics for each poloidal mode for the electrostatic mode shown in Fig. 3 for (a) pure ITG with adiabatic electron response and (b) ITG-TEM without nonadiabatic passing electrons.

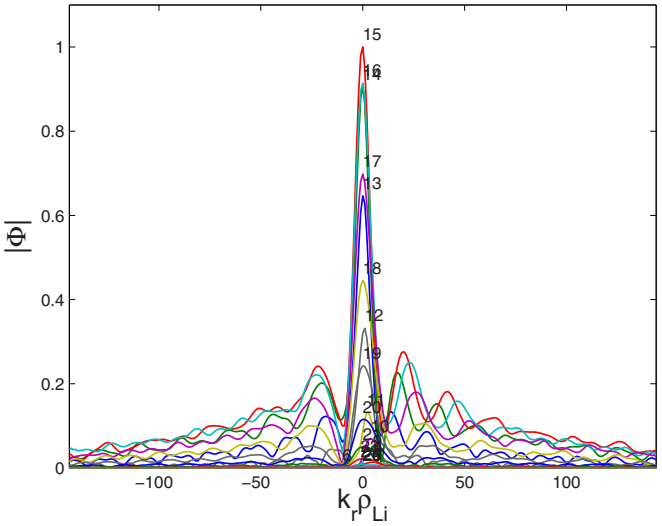

FIG. 7. (Color online) Radial Fourier harmonics for each poloidal mode for the electrostatic mode shown in Fig. 3(c) for ITG-TEM with nonadiabatic passing electrons at $\eta_e(s_0)=2.0$.

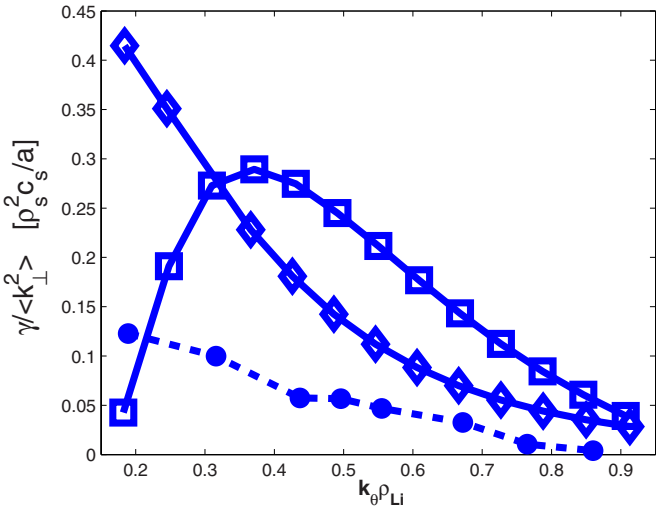

FIG. 9. (Color online) Mixing length estimate for transport coefficient $D_{ML}=\gamma/\langle k_\perp^2\rangle$ in gyro-Bohm units as a function of $k_\theta\rho_{L_i}$; $\eta_i(s_0)=2$ for (a) pure ITG with adiabatic electron response (solid line with squares), (b) ITG-TEM without nonadiabatic passing electrons (divided by 8) (solid line with diamonds), and (c) ITG-TEM with nonadiabatic passing electrons at $\eta_e(s_0)=2$ (dashed line with filled circles).

without nonadiabatic passing electrons, and in Fig. 7 for the ITG-TEM with nonadiabatic passing electrons. Figure 8 documents the mode-averaged measure of $k_\perp$ along with its two components k_θ and k_r for the three cases. The introduction of trapped electrons to the ITG-adiabEl mode and then nonadiabatic passing electrons to ITG-TEM enhances the effective $k_\perp$ by bringing multiscale structures. Because of the increase in the mode-averaged perpendicular wave number $k_\perp$, one requires more radial mode numbers for good resolution as well as convergence (Fig. 7). Since the effect of the nonadiabatic passing electrons is to introduce short multiscale structures into the global eigenmode, thereby increasing effective $k_\perp$, one would like to see how it can affect the

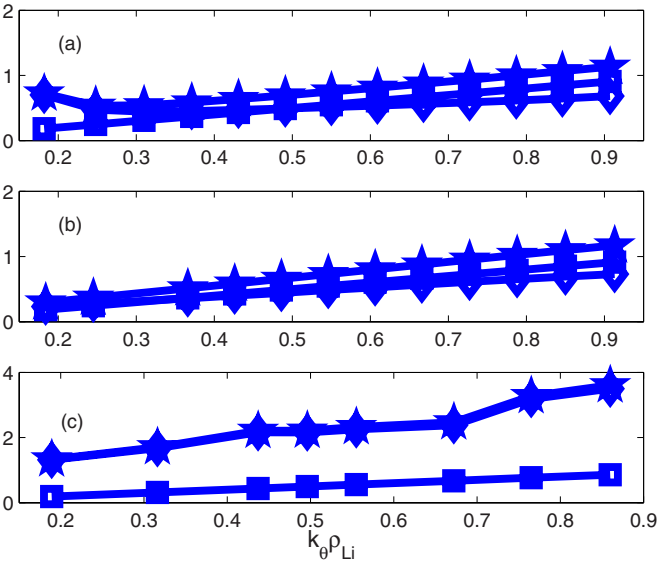

FIG. 8. (Color online) Eigenmode-averaged normalized mode numbers $\langle k_\theta\rho_{L_i}\rangle$ (squares), $\langle k_r\rho_{L_i}\rangle$ (diamonds), and $\langle k_\perp\rho_{L_i}\rangle$ (stars) at $\eta_i(s_0)=2$: (a) pure ITG with adiabatic electron response, (b) ITG-TEM without nonadiabatic passing electrons, and (c) ITG-TEM with nonadiabatic passing electrons at $\eta_e(s_0)=2.0$.

transport. Here we use the simple mixing length estimation for transport coefficient, where one requires calculating the parameter $\mathcal{D}_{ML}=\gamma/\langle k_\perp^2\rangle$, with γ and $\langle k_\perp^2\rangle$ being the growth rate and mode averaged square of perpendicular wave number, respectively. This $\mathcal{D}_{ML}$ is here plotted in gyro-Bohm units in Fig. 9 against $k_\theta\rho_{L_i}$. While the transport coefficient first increases with $k_\theta\rho_{L_i}$ and peaks at $k_\theta\rho_{L_i}=0.4$ and then starts falling for ITG-adiabEl, it, on the other hand, decreases monotonically with $k_\theta\rho_{L_i}$ for ITG-TEM without nonadiabatic passing electron response. To note that the $\mathcal{D}_{ML}=\gamma/\langle k_\perp^2\rangle$ in this case is divided by 8 to show it in the same figure. The inclusion of nonadiabatic passing electron physics into ITG-TEM reduces the transport but keeps the dependence on $k_\theta\rho_{L_i}$ same. Since the radial length scale of perturbation is shortened as is apparent from Fig. 4, the step size over which particles and energy can be thrown away is reduced. This leads to the decrease in the transport coefficient for the ITG-TEM with nonadiabatic passing electron response below the ITG-adiabEl level.

An η_i scan for fixed $\eta_e=2.0$ for the three cases is documented in Fig. 10. The ITG-adiabEl mode becomes weaker and weaker as η_i is decreased and finally subsides. ITG-TEM without nonadiabatic passing electrons, on the other hand, transforms itself from dominantly ITG mode to dominantly TEM, as one reduces η_i. The reason is that with decreasing η_i, the free energy that drives the ITG mode becomes lesser and lesser, but the finite η_e provides the free energy to the trapped electrons so that mode inherent to trapped electrons starts becoming unstable. The transition occurs at $\eta_i\sim 1.6$. Nonadiabatic passing electrons resist the transition of the mode from ITG to TEM character and retain the real frequency in the ion diamagnetic direction with no critical η_i.

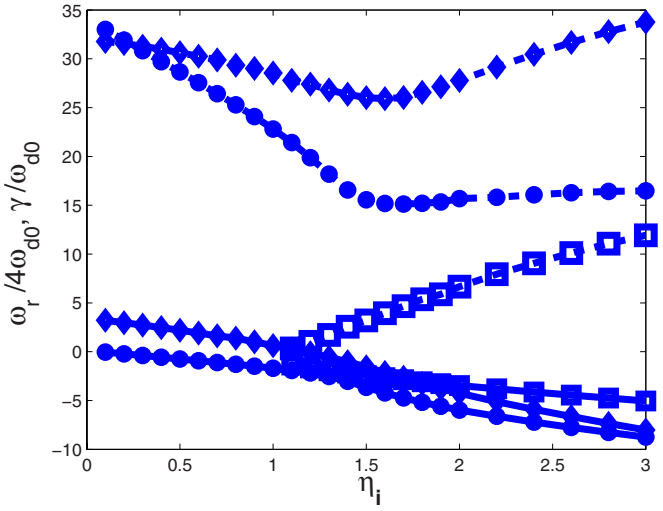

FIG. 10. (Color online) Growth rate $\tilde{\gamma}$ and real frequency $\tilde{\omega}_r$ vs η_i at $\eta_e(s_0)=2$ (i) for pure ITG with adiabatic electrons (squares), (ii) ITG-TEM without nonadiabatic passing electrons (diamonds), and (iii) ITG-TEM with nonadiabatic passing electrons (filled circles).

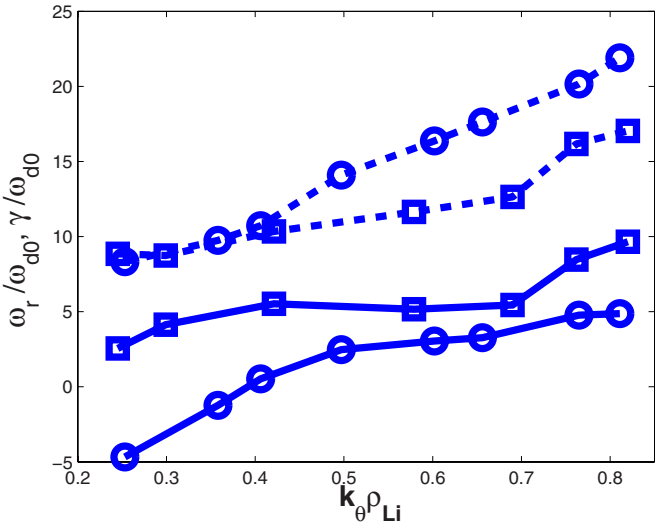

FIG. 11. (Color online) Growth rate $\tilde{\gamma}$ (dashed line) and real frequency $\tilde{\omega}_r$ (solid line) for $\eta_i(s_0)=2$ (i) for pure TEM without nonadiabatic passing electron model (squares) and (ii) pure TEM with nonadiabatic passing electron model at $\eta_i(s_0)=\eta_e(s_0)=2.0$ (open circles).

B. Pure TEM

TEMs are sustained by the trapped electron population in the bad-curvature region of a tokamak. Similar to the passing particles, the trapped particles can also produce unstable modes in the presence of density or temperature inhomogeneities. TEM produced due to the presence of electron density gradient is driven by charge separation, while that produced due to the presence of ETG is driven by compressibility. The passing fraction of electrons, when considered to respond adiabatically, can maintain the growth rate at a lower value. Recently, TEM in the presence of passing electrons has been studied nonlinearly in Ref. 16 which shows the signature of the persistence of the linear mode structure in the nonlinear regime. Here we shall show that the nonadiabatic fraction of passing electrons significantly alters the stability properties of TEM.

We start with the $k_\theta \rho_{L_i}$ scan of the real frequency and growth rate normalized by $\omega_{d0}=v_{\mathrm{th}_i}(s=s_0)\varrho_{L_i}/a^2$ for the TEM for two cases, namely, (i) TEM without nonadiabatic passing electrons and (ii) TEM with nonadiabatic passing electrons in Fig. 11. The dashed line with squares represents the growth rate for case (i), while the solid line with squares represents the corresponding real frequency. The dashed line with open circles is for growth rate for case (ii), with solid lines with open circles representing the corresponding real frequency. The scan reveals that nonadiabatic passing electrons destabilizes the TEM further. TEM whether produced due to density gradient or temperature gradient has EXB drift at its root. When one considers passing electrons to be adiabatic, the moment charge separation is produced; these electrons move to the region of finite charge separation and wipe out the space charge, thus denying the possibility of building up of EXB advection or reducing it. Nonadiabatic passing electrons, on the other hand, take finite time, especially near the $k_\parallel=0$ surfaces, to reach the region of EXB advection, thereby allowing finite time for the mode to grow. TEM thus gets enhanced when one considers the fraction of nonadiabatic passing electrons. One can expect similar effect of nonadiabaticity of passing electrons on density gradient driven TEM also.

Next we look at the change in the mode structures of TEM in the presence of these electrons. The global mode structures for the two cases without and with nonadiabatic passing electrons are shown in Fig. 12 with a close-up view presented in Fig. 13. It is clear that the modes span through several mode rational surfaces. Nonadiabatic passing electrons have strong effect near these surfaces, leading to a strong rise in the radial perturbed electric field. This breaks up the mode structure at these surfaces. Similar to the ITG-TEM case, the mode rotates toward the good-curvature region. The local rise in the perturbed radial electric field near mode rational surfaces becomes clear when one looks at the potential amplitude across the minor radius, corresponding to different poloidal harmonics in Fig. 14, without and with nonadiabatic passing electrons. Strong poloidal coupling is well demonstrated in both cases where at each radial position the mode has contribution from several neighboring compo-

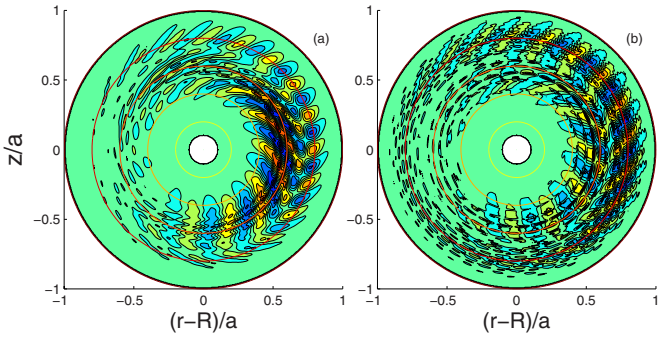

FIG. 12. (Color online) Two dimensional eigenmode structure for (a) TEM without nonadiabatic passing electron response and (b) TEM with nonadiabatic passing electron response at $n=7$ and $\eta_i(s_0)=\eta_e(s_0)=2$.

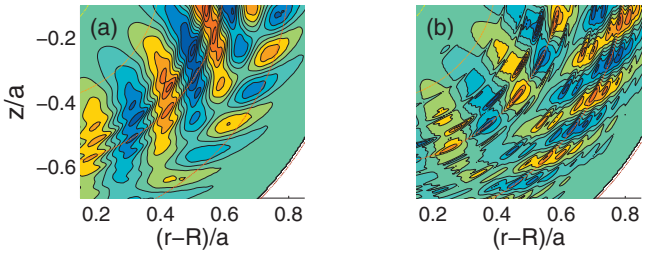

FIG. 13. (Color) Closeup of two dimensional eigenmode structure of (a) TEM without nonadiabatic electron response and (b) TEM with nonadiabatic passing electron response for $n=7$ and $\eta_i=2(s_0)$, $\eta_e=2(s_0)$.

nents. Figures 15 and 16 document the potential in the Fourier space for the two cases. Production of short scales in the eigenmode structure rises the effective averaged $k_\perp$ from the adiabatic passing electron case to nonadiabatic passing electron case, as can be seen in Fig. 17. Estimation of transport via electron channel for which TEM is believed to be an obvious candidate is shown in Fig. 18 using simple mixing length estimation, where $\mathcal{D}_{ML}=\gamma/\langle k_\perp^2\rangle$ is plotted in gyro-Bohm units versus $k_\theta\rho_{L_i}$. The transport coefficient decreases monotonically with increasing $k_\theta\rho_{L_i}$ for both cases. However, $\mathcal{D}_{ML}$ is reduced when one introduces a nonadiabatic fraction of passing electrons to the adiabatically responding passing electron TEM. The reduction in the transport similar to the ITG-TEM case can be understood as due to decreased transport step size caused by the nonadiabaticity of passing electrons.

IV. CONCLUSION

We have investigated the effects of nonadiabaticity of passing electrons on ITG-TEM and TEM using a global gyrokinetic spectral code EM-GLOGYSTO. The model includes both passing and trapped particles, profile variations, true ion to electron mass ratio, arbitrary order FLR effects, transit/trapped particle resonances, and poloidal and radial coupling. A comprehensive description of ITG, ITG-TEM, and pure

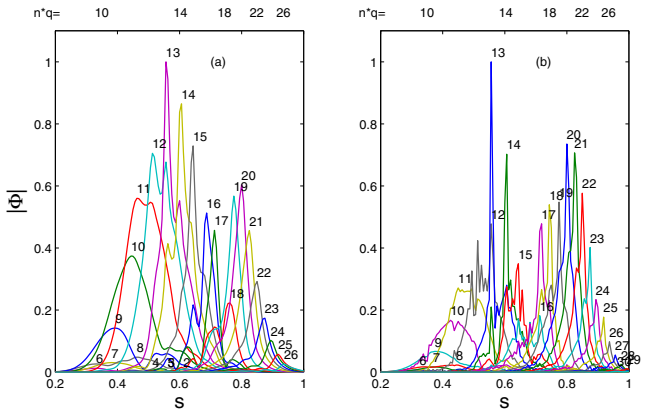

FIG. 14. (Color online) Poloidal Fourier components for electrostatic mode shown in Fig. 12. Note that at each radial location, there are several poloidal harmonics coupled. A few locations where $k_{\|m,n}=0$ (i.e., $nq=m$) are indicated on the top axis. Nonadiabatic electrons introduce sharp structure near these points.

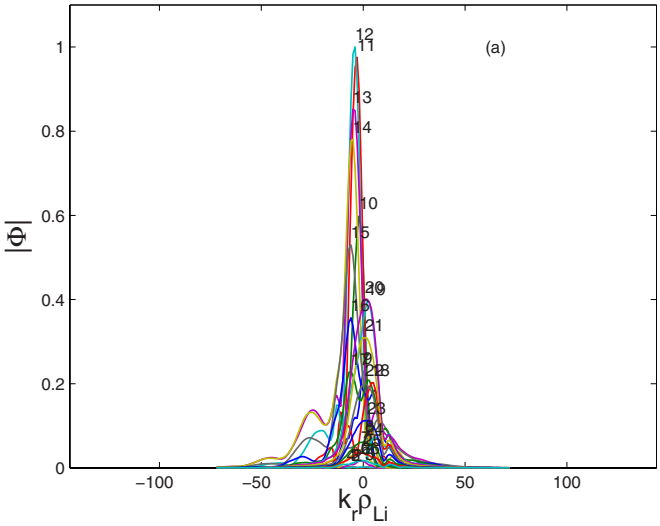

FIG. 15. (Color online) Radial Fourier harmonics for each poloidal mode for the electrostatic mode shown in Fig. 12(a) for TEM without nonadiabatic passing electron response.

TEM including all relevant species is presented. The major findings are as follows.

(1) For the low n or global modes, nonadiabatic passing electrons stabilize the ITG-TEM. However, it has deleterious effect on pure TEM leading to an increase in the growth rate.
(2) For both ITG-TEM and TEM, the spatial mode structures exhibit multiscale feature. Because of the drastic rise in the phase velocity near the $k_\|=0$ surfaces, passing electrons fail to respond adiabatically near these surfaces, leaving open charge separation and pronounced EXB drift. This breaks up the mode structure near the $k_\|=0$ surfaces.

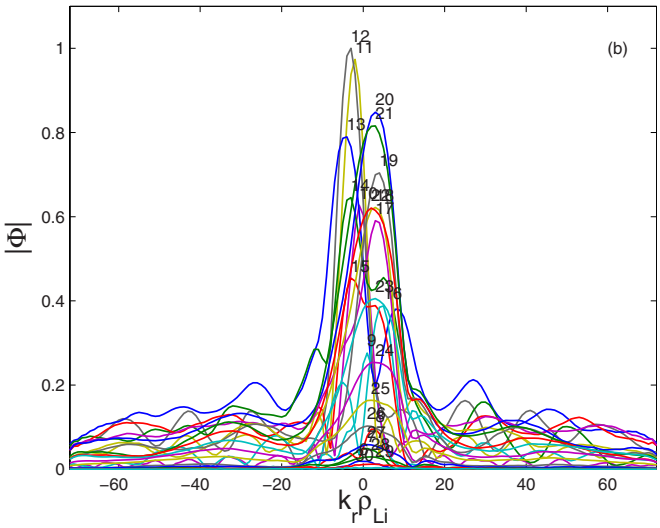

FIG. 16. (Color online) Radial Fourier harmonics for each poloidal mode for the electrostatic mode shown in Fig. 12(b) for TEM with nonadiabatic passing electron response. For numerical convergence we have tested with larger number of radial harmonics and observed that the results are converged (not shown).

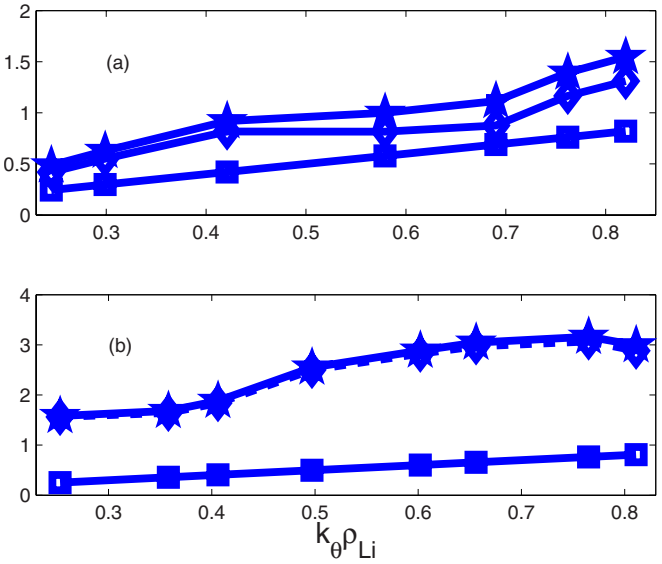

FIG. 17. (Color online) Eigenmode-averaged normalized mode numbers $\langle k_\theta \rho_{L_i} \rangle$ (squares), $\langle k_r \rho_{L_i} \rangle$ (diamonds), and $\langle k_\perp \rho_{L_i} \rangle$ (stars) as a function of $k_\theta \rho_{L_i}$ at $\eta_i(s_0)=2$: (a) TEM without nonadiabatic passing electron response and (b) TEM with nonadiabatic passing electrons at $\eta_e(s_0)=2.0$.

(3) The existence of multiscale features in the spatial mode structure makes effective $k_\perp$ higher, which eventually reduces the mixing length based estimation of transport of the corresponding modes below the level predicted by their respective adiabatic electron models.

As is observed, a mixing length based estimate leads to an important reduction in diffusivity. Nonlinear global simulations will be necessary to confirm this fact, considering that there are situations where nonlinear effects tend to introduce larger scales, e.g., in the case of inverse cascades and where mixing length estimates have proven wrong.

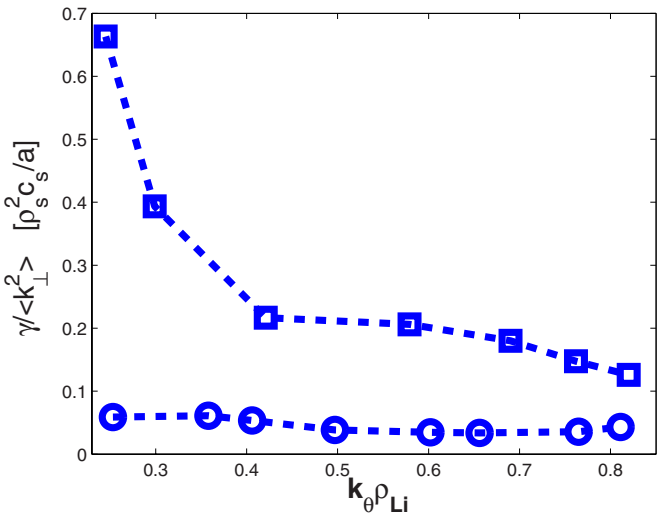

FIG. 18. (Color online) Mixing length estimate for transport coefficient $D_{ML}=\gamma/\langle k_\perp^2 \rangle$ in gyro-Bohm units as a function of $k_\theta \rho_{Li}$: $\eta_i(s_0)=2$ for (a) pure TEM without nonadiabatic passing electron response (dashed line with squares) and (b) pure TEM with nonadiabatic passing electron response at $\eta_e(s_0)=2$ (dashed line with open circles).

It is perhaps worth noting that a flux-tube model with correct implementation of magnetic shear and boundary conditions along the magnetic field line should also be able to reproduce the fine radial structures at the mode rational surfaces resulting from nonadiabatic passing electron dynamics. However, to our knowledge, such features have not been clearly pointed out in the past literature.

Equilibrium flows, as well as electromagnetic and Shafranov shift effects, can in certain cases be important for the instabilities that were studied in this paper. ETG modes with full electron and ion dynamics is another area of interest. We hope to address some of these issues in future work.

ACKNOWLEDGMENTS

Two of the authors (J.C. and R.G.) are thankful to IPR Computer Centre for its support during the course of this work. The entire computation was performed on a 34-node Xeon cluster with fast-ethernet interconnect at IPR. The CRPP authors were partly supported by the Swiss National Science Foundation.

[1] W. Horton, Rev. Mod. Phys. **71**, 735 (1999).
[2] P. Terry, Rev. Mod. Phys. **72**, 109 (2000).
[3] S. E. Parker, W. W. Lee, and R. A. Santoro, Phys. Rev. Lett. **71**, 2042 (1993).
[4] A. M. Dimits, T. J. Williams, J. A. Byers, and B. I. Cohen, Phys. Rev. Lett. **77**, 71 (1996).
[5] S. Brunner, M. Fivaz, T. M. Tran, and J. Vaclavik, Phys. Plasmas **5**, 3929 (1998).
[6] R. D. Sydora, V. K. Decyk, and J. M. Dawson, Plasma Phys. Controlled Fusion **38**, A281 (1996).
[7] M. A. Beer and G. W. Hammett, Phys. Plasmas **3**, 4018 (1996).
[8] B. H. Fong and T. S. Hahm, Phys. Plasmas **6**, 188 (1999).
[9] W. W. Lee, J. L. V. Lewandowski, T. S. Hahm, and Z. Lin, Phys. Plasmas **8**, 4435 (2001).
[10] C. Z. Cheng, Nucl. Fusion **22**, 773 (1982).
[11] A. J. Redd, A. H. Kritz, G. Bateman, G. Rewoldt, and W. M. Tang, Phys. Plasmas **6**, 1162 (1999).
[12] P. Malinov and F. Zonca, J. Plasma Phys. **71**, 301 (2005).
[13] B. B. Kadomtsev and O. P. Pogutse, Nucl. Fusion **11**, 67 (1971).
[14] M. N. Rosenbluth and M. L. Sloan, Phys. Fluids **14**, 1725 (1971).
[15] P. C. Liewer, Nucl. Fusion **25**, 543 (1985).
[16] T. Dannert and F. Jenko, Phys. Plasmas **12**, 072309 (2005).
[17] D. W. Ross, R. V. Bravenec, W. Dorland, M. A. Beer, G. W. Hammett, G. R. McKee, R. J. Fonck, M. Murakami, K. H. Burrell, G. L. Jackson, and G. M. Staebler, Phys. Plasmas **9**, 177 (2002).
[18] D. W. Ross and W. Dorland, Phys. Plasmas **9**, 5031 (2002).
[19] R. E. Waltz, J. M. Candy, and M. N. Rosenbluth, Phys. Plasmas **9**, 1938 (2002).
[20] J. Candy and R. E. Waltz, J. Comput. Phys. **186**, 545 (2003).
[21] J. Candy and R. E. Waltz, Phys. Rev. Lett. **91**, 045001 (2003).
[22] Y. Chen, S. E. Parker, B. I. Cohen, A. M. Dimits, W. M. Nevins, D. Shumaker, V. K. Decyk, and J. N. Leboeuf, Nucl. Fusion **43**, 1121 (2003).
[23] A. M. Dimits, G. Bateman, M. A. Beer, B. I. Cohen, W. Dorland, G. W. Hammett, C. Kim, J. E. Kinsey, M. Kotschenreuther, A. H. Kritz, L. L. Lao, J. Mandrekas, W. M. Nevins, S. E. Parker, A. J. Redd, D. E. Shumaker, R. Sydora, and J. Weiland, Phys. Plasmas **7**, 969 (2000).
[24] R. E. Waltz, J. Candy, and M. Faheyc, Phys. Plasmas **14**, 056116 (2007).
[25] F. Jenko, Comput. Phys. Commun. **125**, 196 (2000).
[26] T. Gorler and F. Jenko, Phys. Rev. Lett. **100**, 185002 (2008).
[27] J. Chowdhury, R. Ganesh, P. Angelino, J. Vaclavik, L. Villard, and S. Brunner, Phys. Plasmas **15**, 072117 (2008).
[28] G. L. Falchetto, J. Vaclavik, and L. Villard, Phys. Plasmas **10**, 1424 (2003).
[29] R. Ganesh, P. Angelino, J. Vaclavik, and L. Villard, Phys. Plasmas **11**, 3106 (2004).
[30] P. Angelino, Ph.D. thesis, EPFL, 2006.

[31]R. Ganesh, J. Vaclavik, and L. Villard, in *Proceedings of the Joint Varenna-Lausanne International Workshop on Theory of Fusion Plasmas*, Villa Monastero-Varenna, Italy, August 2004, edited by J. W. Connor, O. Sauter and E. Sindoni (Societa Italiana Di Fisica, Varenna, Italy, 2004).
[32]P. Angelino, A. Bottino, G. Falchetto, R. Ganesh, J. Vaclavik, and L. Villard, Transp. Theory Stat. Phys. **34**, 333 (2005).
[33]R. Ganesh and J. Vaclavik, Phys. Rev. Lett. **94**, 145002 (2005).
[34]S. Brunner, Ph.D. thesis, EPFL, 1997.